International Journal of Concrete Structures and Materials

Bond Behavior of Basalt Fiber-Reinforced Polymer Bars Embedded in Concrete Under Mono-tensile and Cyclic Loads

Xia Liu[1,2], Xin Wang[2*], Kangyu Xie[3], Zhishen Wu[2] and Feng Li[1]

Abstract

This study evaluates the static and fatigue bond behavior in basalt fiber-reinforced polymer (BFRP) bars embedded in concrete. For bond behavior under a mono-tensile load, BFRP bars with four types of surface patterns (round, rectangular, cross-winding, and spiral-winding) were adopted, and 20 groups of rib parameters were introduced for round-type BFRP bars. The bond–slip relationships and the influences of the above parameters on bond behavior were investigated. An analytical model for simulating the relationships of full bond slip was studied by data fitting. For bond behavior under cyclic loads, the relationship between stress levels and the number of cycles was investigated, and the slip of round-ribbed BFRP bars was studied with respect to the number of cycles. The results showed that the rectangular, cross-winding, and spiral-winding ribbed bars experienced serious wear, and that the average bond strength was approximately 80.6% of that of the round-ribbed bars. Thus, the bond behavior of the round rib is superior to those of the other surfaces. In addition, a bond–slip constitutive model for a BFRP bar is proposed, representing four main stages: a micro-slip stage, a slip stage, a descending stage, and a residual stage. Under cyclic loads, an equation was proposed for predicting fatigue life with a regression coefficient of 0.880, and a development law of slip was characterized as three stages: the linear increase stage, the steady increase stage, and the sharp increase stage, respectively.

Keywords: basalt fiber-reinforced polymer (BFRP), rib parameters, bond behavior, bond–slip constitutive law, fatigue life

1 Introduction

Fiber-reinforced plastic (FRP) bars have been applied to concrete structures, as they exhibit a high strength-to-weight ratio, are non-electromagnetic, and have excellent corrosion resistance (Wu et al. 2007; Keller 2003). FRP bars can be advantageously used in reinforced concrete buildings, bridges, retaining walls, underwater and underground tunnels, roadways, and other structures (Hollaway 2010; Chaallal 1993). In particular, when steel rebar of structures are exposed to corrosive environments, corrosion and deterioration are accelerated (Saito 2002). Therefore, the FRP bar, with its high strength and excellent corrosion resistance, could possibly be set as the reinforcement instead of steel rebar, and also could improve the service life and decrease the maintenance cost during the whole life cycle of the structure.

The bond behavior between bar and concrete is a critical aspect of the structural behavior for any type of reinforcement, including FRP reinforcement. However, the bond between the FRP bar and concrete differs from the well-known properties of steel-reinforced concrete, and the bond mechanism of structures with FRP-reinforced bars in practical engineering is complex. Such complexity arises from the differences in load bearings, development of cracks, and failure modes of concrete structures,

*Correspondence: xinwang@seu.edu.cn
[2] Key Laboratory of C & PC Structures Ministry of Education, Southeast University, Nanjing 210096, Jiangsu, China
Full list of author information is available at the end of the article

Liu *et al. Int J Concr Struct Mater*   (2020) 14:19

Page 2 of 15

and from the significant variations of FRP material with different fiber categories (such as carbon, glass, aramid, and polyvinyl alcohol), outer surface shapes, treatments (e.g., ribbed, indented, or braided bars), bond lengths, bar diameters, and so on. Achillides and Pilakoutas (2004) found that no significant difference was found between the bond strengths developed by GFRP and CFRP bars, which were 8.9 MPa and 9.0 MPa respectively. Aramid and hybrid development bars showed slightly lower bond strengths of 5.4 MPa. Malvar et al. (2003) carried out tensile and bond tests for carbon fiber reinforced polymer (CFRP) rebars. They found that bars with molded external deformations mimic those of steel rebar exhibited a bond strength of 10.1 MPa, bar with small deformation (0.0025 mm or 0.001 in high) was only 3.59 MPa. Cosenza et al. (1999) studied bond behavior of GFRP bar. They reported a bond strength of 14.5 MPa at a slip of 0.25 mm with an embedment length of about 10 days (bar diameter). Straight FRP rods (smooth rods, grain-covered and sandblasted rebar) were compared with deformed FRP rods (ribbed, indented, twisted, sand braided) (Cosenza et al. 1997), results indicated that braided and sanded bars exhibited the best bond strength of 17.78 MPa, grain covered came next with a strength of 12.05 MPa. It is clear that bond behavior was primarily depend on the shape of outer surface. Darwin and Graham (1993) explored effect of deformation pattern (height and spacing) on bond strength of steel bars. The relative area (ratio of projected rib area normal to bar axis to product of nominal bar perimeter and center-to-center rib spacing) was introduced to evaluate combinations of rib height and spacing. The bond strength of FRP bars with rib height, spacing and rib width adopts the ratio in this paper. Malvar et al. (2003) found that bond stress can be increased 2.5 times to about 10 MPa (1450 psi) by varying the confining pressure from 3.45 to 24.1 MPa (500–3500 psi). The importance of lateral confinement has also been discussed by other researchers (Cox and Herrmann 1992; Cox and Guo 1999). Barena et al. (2009) carried out experimental study of bond behavior between concrete and FRP bars using a pull-out test. The experimental results confirm the tendency of rebars with larger diameters to have lower bond strength while the initial stiffness is not mainly influenced by the rebar diameter. Caro et al. (2017) conducted experimental studies on the bonds of FRP bars with parameters of embedment length, FRP bar type and diameter, concrete compressive strength and hole diameter. They found that increase in bar diameter from 10 to 12 mm led to a 30.4% increase in the pull-out capacity and 9.2% decrease in the maximum average bond stress for the specimens with DE CFRP bars. The behavior of the corresponding specimens with DE GFRP bars were not affected by the change in

bar diameter. Tekle et al. (2017) conducted experiments on bond behavior of GFRP reinforcement in alkali activated cement concrete. Results showed that GFRP reinforced AAC concrete has a similar bond–slip curve with GFRP reinforced OPC concrete. Achillides and Pilakoutas (2004) reported that the mode of bond failure of FRP bars in most cases differs from the mode of bond failure of steel deformed bars. Under the condition of adequate confinement of bars, shear cracks develop between steel bar ribs and surrounding concrete while bond failure occurs partly on the surface of the FRP bar.

Most of the conducted studies have focused on the bond behavior of steel bars, carbon fiber-reinforced polymer (CFRP), glass fiber-reinforced polymer (GFRP) and aramid fiber-reinforced polymer (AFRP) bars, only a few experimental studies have been conducted on bond behavior between a basalt fiber-reinforced polymer (BFRP) bar and concrete. In recent decades, the BFRP bar has appeared promising, owing to its high performance-to-cost ratio (compared to CFRP) and high corrosion resistance (compared to GFRP), and it is also an environmentally friendly-material, as the fiber is pulled over a roller with neither precursors nor additives in the manufacturing process (Lopresto et al. 2011; Torres et al. 2013). Thus, the application of a BFRP bar can also benefit the sustainable development of construction. Nowadays, BFRP bars with outer surface shapes with round, rectangular, cross winding, and spiral winding ribs are produced by machines, with high efficiency and high quality. To make full use of their excellent properties, sufficient studies need to be conducted to determine a rational approach to the design of structures reinforced with BFRP bars, particularly in the ductility design of seismic structures. In addition, there is a primary need to explore more influencing factors and to develop constitutive laws for the BFRP bar, i.e., a new theory for the design of reinforced structures with BFRP bars needs to be developed.

For this purpose, a wide range of bond tests are performed to examine bond strength, slip, and different failure modes, to investigate how different types of rib parameters interact with concrete. A comparison of failure modes and bond–slip behavior between BFRP bars and steel reinforcement is performed, and the resisting mechanism activated in the pull-out tests is realized. Subsequently, bond–slip constitutive laws are determined and a fitting is obtained for a BFRP bar, and rational approaches are proposed to forecast the bond performance, and to design the ductility of structures reinforced with BFRP bar. In addition, the long-term bonds between BFRP bars and concrete under cyclic loads are studied, to produce an alternative way to forecast fatigue life and to better understand the increase

Liu *et al. Int J Concr Struct Mater* (2020) 14:19

Page 3 of 15

of local deformation, the decrease of stiffness, and early failure in practical engineering.

2 Test Program

2.1 Parameters of Test Specimen

For monotonic tests and cyclic tests, specimens adopt the same design characteristics based on the code of Japan, with an FRP bar with a diameter smaller than 17 mm, and with the side length of concrete cube specimen recommended to be set to 100 mm (Japan Society of Civil Engineering 1995). The bond length is advised to be four times or more than the diameter, as the bond stress within this length range could be approximately considered as an average distribution. Therefore, in this study, a BFRP bar with diameter of 12 mm and a concrete cube with a size of 100 mm × 100 mm × 100 mm are chosen as shown in Fig. 1, where the bond length is set to 5*d* (*d* is the bar diameter, and thus the bond length is 60 mm). A debond length of 40 mm is selected; this denotes the distance between the concrete and the PVC plastic tube, which is sealed with resin at the top end to fix the bar.

2.1.1 Concrete

Six groups of casting were made during the period of research. Concrete grade of C30 was adopted, in which the largest diameter of coarse aggregate is 20 mm. The grade of ordinary Portland cement is R32.5, the ratio of water to cement is 0.5. The compressive strengths of concrete (f_{cu}) for each batch of pullout tests are shown in Table 4.

2.1.2 BFRP Bar

As shown in Fig. 2, the BFRP bar adopted in this study can be classified with different surface shapes, e.g., as a round rib, rectangular rib, cross-winding rib and spiral-winding rib, and a steel rebar with crescent rib is also introduced. The BFRP bars are produced automatically, by pultrusion with a basalt fiber volume of 70% and vinyl ester resin volume of 30%. The mechanical properties of the rebar are shown in Table 1.

In fact, the round rib was made from a spiral indentation in the bar that results from a spiral strand wrapped around the outside diameter, whereas the rectangular rib was machined by intervals of cutting off continuous longitudinal basalt fiber bound with a lathe. The cross-winding and spiral-winding ribbed bars are pultruded
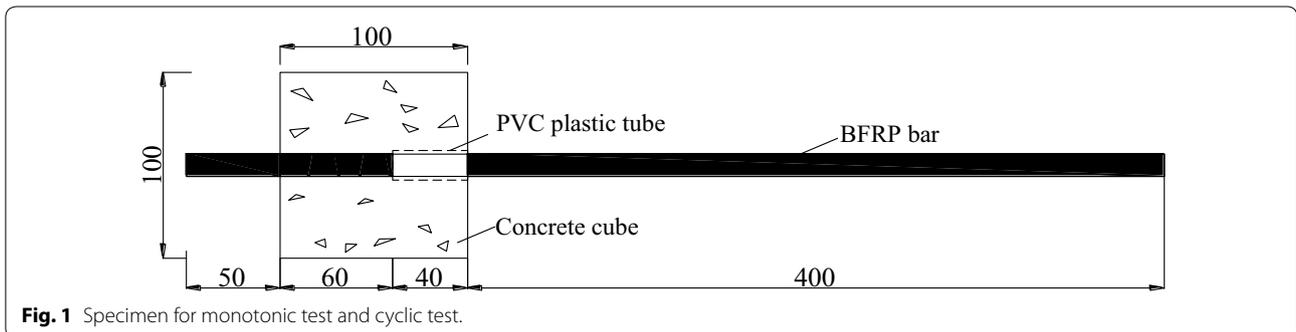
Fig. 1 Specimen for monotonic test and cyclic test.

a Round rib

b Rectangular rib

c Cross-winding rib

d Spiral-winding rib

e Steel rebar with crescent rib
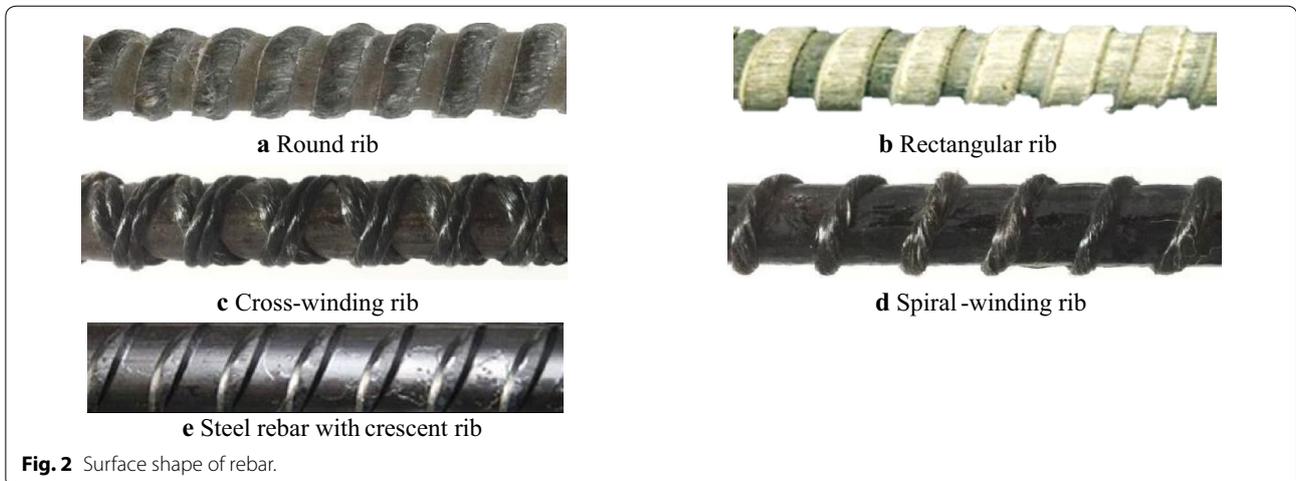
Fig. 2 Surface shape of rebar.

Liu *et al. Int J Concr Struct Mater*   (2020) 14:19

Page 4 of 15

Table 1 Measured mechanical properties.

Type	Nominal diameter/ mm	Density/(g/cm³)	Elastic modulus/ GPa	Yield strength/ MPa	Tensile strength/ MPa	Elongation/%
BFRP bar	12	2.1	55	–	1208	2.5
Steel rebar	12	7.8	195	425	–	15

with a smooth surface, around which cross strands or spiral strands are wrapped and glued with polyester resin. Moreover, 20 groups of rib parameters including the shape, height (H_R), space (S_R), and width (W_R) are introduced in Table 2. For monotonic tests, a total of 60 bars are investigated with three specimens in each group. Based on previous researches (Darwin and Graham 1993), relative rib area R_r is an appropriate parameter to evaluate effect of deformations on bond strength of steel bars. R_r is introduced to evaluate effect of BFRP bar rib on bond strength.

$$R_r = \frac{projected\ rib\ area\ normal\ to\ bar\ axis}{nominal\ bar\ perimeter \times rib\ space} \quad (1)$$

2.2 Test Setup
As shown in Fig. 3, the specimen is fixed in the hanging basket; the BFRP bar passes through the preformed hole in the lower plate of the hanging basket and is clamped by the lower pair of clamps of the machine. During the process of loading, the machine moves upward or downward, and BFRP bar can achieve free rotation in the preformed hole so as to maintain the pull-out force in the axial direction. To measure the slip at the loaded end, a linear variable differential transformer (LVDT) rack is set at the clamping end of the specimen, and keeps the same horizontal position as the initial position of debonding of the BFRP bar. Two LVDTs are fixed at both the left and right sides, so the tilt deviation during the loading process can be eliminated by their mean value. The displacement at the free end of the specimen is measured using the upper LVDT.

2.3 Loading System
For the mono-tensile test, testing machines produced by the Swiss Walter + Bai Company are adopted, with the accuracy of grade 0.5. Unidirectional tension is

Table 2 Parameters of specimens.

Series	Rib shape	Number	Height/mm (H_R)	Space/mm (S_R)	Width/mm (W_R)	Relative rib area (R_r)
I	Round	B-r-0.84-9-1.5	0.84	9	1.5	0.093
		B-r-0.84-9-2.5	0.84	9	2.5	
		B-r-0.84-9-4	0.84	9	4	
		B-r-0.84-12-1.5	0.84	12	1.5	0.070
		B-r-0.84-12-2.5	0.84	12	2.5	
		B-r-0.84-12-4	0.84	12	4	
		B-r-0.84-18-2.5	0.84	18	2.5	0.047
		B-r-0.84-18-4	0.84	18	4	
		B-r-1.08-9-1.5	1.08	9	1.5	0.120
		B-r-1.08-9-2.5	1.08	9	2.5	
		B-r-1.08-9-4	1.08	9	4	
		B-r-1.08-12-1.5	1.08	12	1.5	0.090
		B-r-1.08-12-2.5	1.08	12	2.5	
		B-r-1.08-12-4	1.08	12	4	
		B-r-1.08-18-2.5	1.08	18	2.5	0.060
		B-r-1.08-18-4	1.08	18	4	
II	Rectangular	B-rec-0.84-12-4	0.84	12	4	
III	Crossing winding	B-cw-0.84-12-4	0.84	12	4	
IV	Spiral winding	B-sw-0.84-12-4	0.84	12	4	
V	Crescent	S	–	–	–	–

B-r-0.84-9-1.5 indicates: B, the BFRP bar; r, round rib; 0.84, the rib height; 9, the rib spacing, 1.5, the rib width.

Liu *et al. Int J Concr Struct Mater*   (2020) 14:19

Page 5 of 15
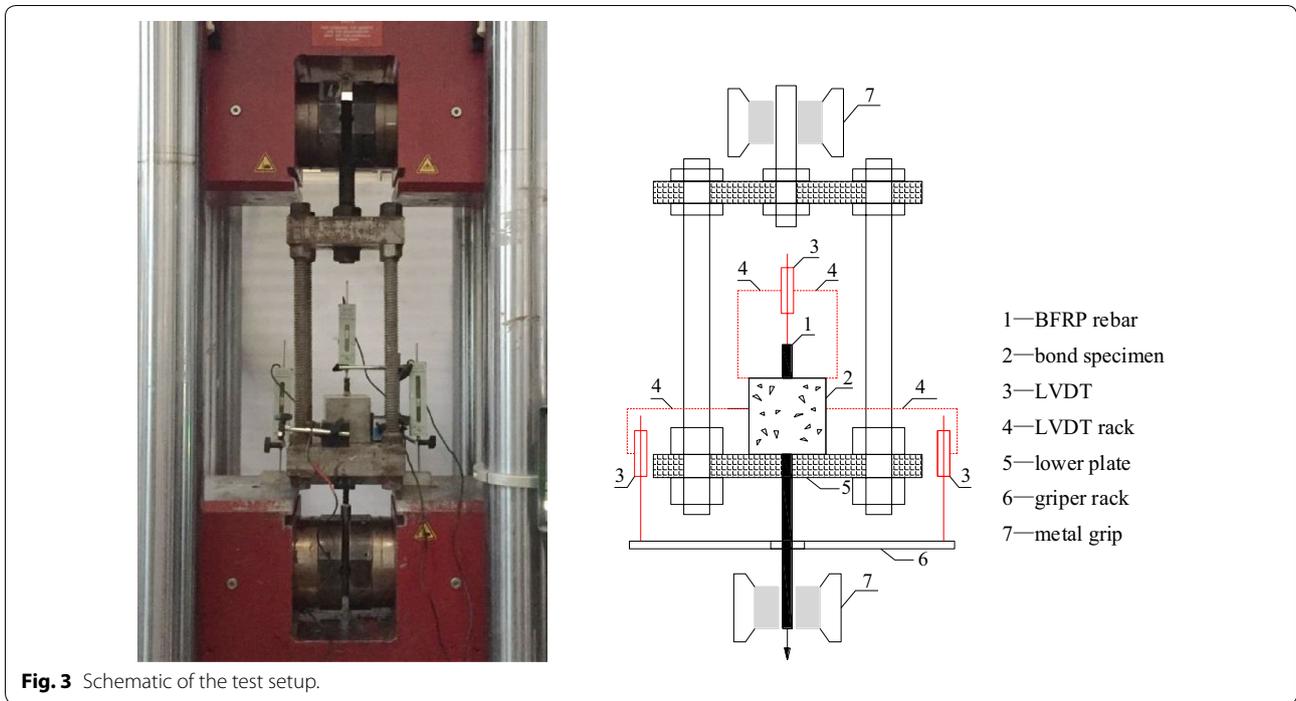
Fig. 3 Schematic of the test setup.

adopted with a stroke speed of 0.75 mm/min, which is smaller than the displacement controlling speed of 1.3 mm/min stipulated by ACI standards (ACI 440.3R-04 2004). The force sensor of the machine records the force at the loaded end; the slips at loaded end and unloaded end are recorded by the three LVDTs. The data were collected via data logger DH 3816 N provided by Donghua Testing Technology Co., Ltd.

With the same test setup, the round-ribbed BFRP bars were selected to conduct the study on fatigue behavior under cyclic loads. The fatigue tests are carried out at a frequency of 5 Hz according to the guidelines of the Japan Society of Civil Engineers (JSCE) (1995), and the loading scheme of the stress level (S_l) and the stress ratio (R) are shown in Table 3.

In the above, $S_l = \sigma_{max}/\sigma_u$, σ_{max} was the maximum loading stress, and σ_u was the bond strength, and was set to 22.5 MPa according to the mono-tensile results (Table 4). $R = \sigma_{min}/\sigma_{max}$, and σ_{min} was the minimum loading stress, set to 1/10 of the value of the bond strength.

2.4 Data Process
2.4.1 Slip at Loaded End
As the BFRP bar was embedded in the concrete, its slip could not be measured directly. The slip at loaded end should be calculated by $S = S_m - \delta_e$ (Hao et al. 2009), where S_m is the measuring slip of the BFRP bar by lower

Table 3 Loading scheme of specimen under cyclic load.

Number of specimen	Stress level (S_l)	σ_{max}/MPa	σ_{min}/MPa	R
FB01	0.60	13.5	2.25	0.167
FB1-1, FB1-2	0.65	14.63		0.154
FB2-1, FB2-2	0.68	15.30		0.147
FB3-1, FB3-2	0.73	16.43		0.137
FB4-1, FB4-2	0.75	16.88		0.1333
FB5-1, FB5-2	0.80	18.00		0.125

two LVDTs, which represents bar slip but also the bar elongation. δ_e is the elastic elongation of the BFRP bar above the embedment length.

2.4.2 Bond Strength Under Mono-tensile Load
Based on the literature (Achillides and Pilakoutas 2004; Chaallal and Benmokrane 1993), for concrete strengths less than 15 MPa, the concrete is crushed in front of the bar deformations, and the bond strength is controlled mainly by the shear strength of concrete. For concrete strengths greater than 30 MPa, the bond strength of FRP bars does not appear to be controlled by the concrete strength. A concrete grade of C30 is adopted in this paper and their compressive strengths of each batch are shown in Table 4. Within a bond length of 5d, the bond stress could be considered to be uniform along the embedded length. Therefore, the bond stress

Liu *et al. Int J Concr Struct Mater*   (2020) 14:19

Page 6 of 15

Table 4 Results of pull-out test under mono-tensile load.

Series	Number of specimen	Average pull-out strength/MPa	CV of pull-out strength/%	Average slip* at loaded end/mm	CV of slip*/%	f_{cu} /MPa
I	B-r-0.84-9-1.5	17.30	4.78	2.66	1.24	23
	B-r-0.84-9-2.5	17.54	3.12	2.74	0.89	
	B-r-0.84-9-4	18.10	5.63	1.22	0.82	
	B-r-0.84-12-1.5	18.81	5.82	3.73	2.85	35
	B-r-0.84-12-2.5	17.32	1.70	3.41	15.12	
	B-r-0.84-12-4	19.80	3.55	3.87	6.79	
	B-r-0.84-18-2.5	13.19	3.84	3.96	4.12	27
	B-r-0.84-18-4	12.65	8.32	4.00	2.70	
	B-r-1.08-9-1.5	14.85	0.33	2.93	2.69	29
	B-r-1.08-9-2.5	16.65	1.67	2.67	4.00	
	B-r-1.08-9-4	16.27	3.35	2.40	10.42	
	B-r-1.08-12-1.5	20.00	6.72	3.94	3.72	31
	B-r-1.08-12-2.5	22.50	1.64	3.56	5.82	
	B-r-1.08-12-4	20.01	0.00	3.41	2.09	
	B-r-1.08-18-2.5	11.69	2.37	5.65	2.61	27
	B-r-1.08-18-4	13.15	4.56	3.94	5.09	
II	B-rec-0.84-12-4	11.20	6.12	1.04	8.21	28
III	B-cw-0.84-12-4	13.48	7.09	3.37	4.51	
IV	B-sw-0.84-12-4	13.59	5.03	4.28	7.07	
V	S	11.66	8.20	1.69	0.01	28

The values of ultimate bond strength are the mean of experimental results. Slip* means slip corresponding to max bond stress.

f_{cu} is the compressive strength of concrete.

τ is calculated by dividing the pull-out force P by the surface area of the rebar embedded in the concrete, $\pi d l_d$, where d is the diameter of the BFRP bar, and l_d is the bond length of the BFRP bar.

3 Test Results

3.1 Failure Modes Under Mono-tensile Load

There are mainly two types of failure modes (Figs. 4 and 5). One is a pull-out of the bar, and the other is a split failure of the concrete.

In most cases, rectangular-ribbed, cross-winding-ribbed, and spiral-winding-ribbed bar exhibit overall pull-out failures. The rectangular, cross-winding, and spiral-winding ribs of the BFRP bars are worn away heavily with respect to the round-ribbed bar (Fig. 4). The surface of the rectangular rib is sheared off at a discontinuous fiber, whereas both the cross- and spiral-winding ribs (glued to the bar) are prone to separate from the inner bar, and then to fracture during the pull-out process. In contrast, the round-ribbed BFRP bar and steel

Round   Rectangular   Cross winding   Spiral winding   Steel   Surface of concrete with basalt fiber-reinforced polymer (BFRP) bar   Surface of concrete with steel bar

Fig. 4 Failure modes under mono-tensile load.

a Pull-out of BFRP bar   **b** Split of concrete   **c** fracture of BFRP bar
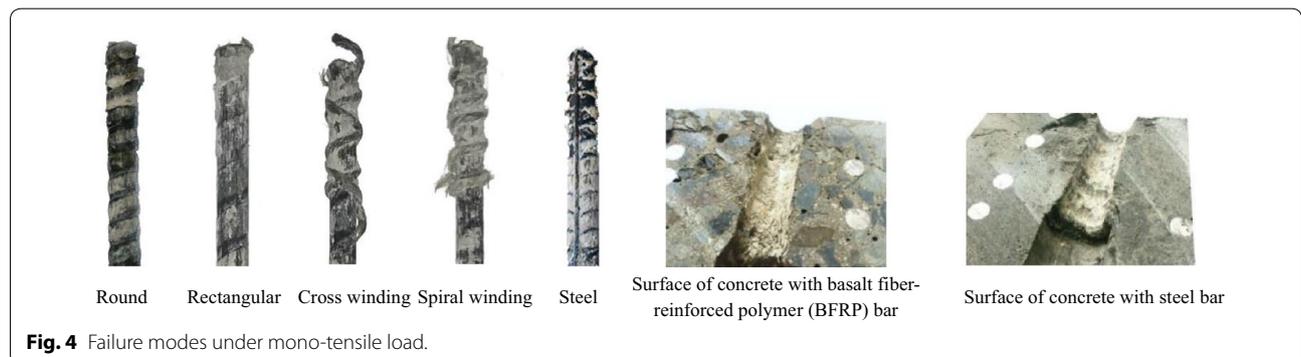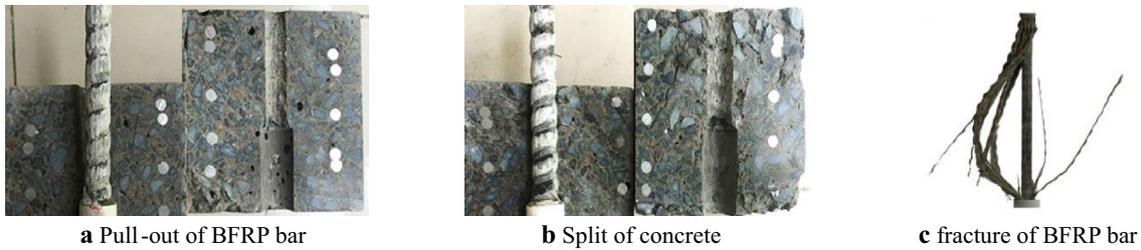
Fig. 5 Failure modes under cyclic loads.

rebar nearly remain in good condition, while the embedded concrete between each two adjacent ribs is seriously shredded. As a detailed observation on the interface with concrete specimens in Fig. 4, the surfaces of the profiles of BFRP bars (rectangular, cross-winding, and spiral-winding ribbed) are nearly flat, whereas those of the round-ribbed bar and steel rebar are evidently rough, with a small amount of concrete shredded and taken out. In rare cases of the ribbed BFRP bar, the concrete experiences a spilt failure, where the rib of the BFRP bar appears to be worn, and the concrete embedded in the rib experiences shear failure.

In conclusion, the round-ribbed BFRP bar possesses the strongest rib strength, as the longitudinal basalt fibers at the rib are continuous, whereas those of the rectangular rib are discontinuous owing to the cutting during the formation of the rib shape. The detach failure of cross-winding and spiral-winding ribs initiates at the bond surface between the fiber bound and the bar surface, owing to the limited contact area and glue strength between the fiber bounds and bar surface. In that regard, all the analysis in this study is based on data that excludes split failure, as this occurs suddenly and leads to brittle bond failure.

3.2 Failure Modes Under Cyclic Loads

The three types of failure modes observed during the cyclic test are the pull-out of bar, the split of the concrete, and the fracture of the bar, respectively.

The first type was characterized as the pull-out of the BFRP bar with no evident cracks on the concrete (Fig. 5a). For specimens FB01, FB1-1, FB1-2 and FB2-1 with relatively low stress levels, the pulled-out bar exhibited a worn rib, while the small amount of concrete embedded between the two adjacent ribs was sheared off. It can be seen from the profile in Fig. 5a that the bond surface against concrete was relatively smooth, which was attributed to the continuous micro-damage accumulation between the BFRP bar and the concrete. It can be concluded that concrete shears the ribs on the surfaces of the BFRP bars under cyclic loads, and that the bond surface was beginning to fail because of the continuous accumulation of damage from the loaded end. Then, the effective bond length was extended to the free end until reaching its lowest limit, abruptly causing a large slip and eventually pulling-out failure.

In the second type of failure mode, the BFRP bar was pulled out but the concrete has evident cracks. This involves the specimens of FB3-1, FB3-2, FB4-1, FB4-2, FB5-1 and FB5-2. For specimens with a higher stress level, a rib with sheared-off concrete indicated such specimens tend to split under cyclic loads. As observed, the cracks initiated at the free end and developed along the bar, then expanded from the interacted surface of the BFRP bar and concrete to the outer surface within a few seconds, and finally and abruptly turned into a longitudinal split crack along the direction of the embedded BFRP bar. As indicated, there is evident bond resistance between the ribs and concrete under higher cyclic loads, and the bond behavior develops primarily from mechanical interlocking.

The third type of failure mode was characterized as fracture of the BFRP bar and was only exhibited in specimen FB2-2 at cycles of 300,000. The delamination of fiber on the external surface against resin caused the fracture of fiber when the tension reaches a peak. Immediately, the fibers of the inner surface were pulled out as a whole. In this regard, fabrication defects of the BFRP bar may cause this type of failure mode.

3.3 Test Results

The experimental results of pull-out tests under a mono-tensile load are shown in Table 4.

In terms of cyclic test, a total of 11 round-ribbed BFRP bars were selected to conduct study on fatigue behavior. In order to research the S−N curve of bond behavior, 6 groups of stress levels were designed. For stress level of 0.60, the specimen FB01 reaches terminal cycles at 2 million, and the specimen without failure is not included in curve fitting. Thus one specimen for FB01 was reasonable. For stress level ranges from 0.65 to 0.80, two specimens for each stress level are adopted. It will be better

Liu *et al. Int J Concr Struct Mater*   (2020) 14:19

Page 8 of 15

Table 5 Results of specimens under cyclic loads.

No.	Cycles	Description of failure	Slip*/mm
FB01	2 million	Terminal cycles was reached	–
FB1-1	30,254	BFRP bar was pull out without obvious cracks on the concrete	4.71
FB1-2	330,000	BFRP bar was pull out without obvious cracks on the concrete	3.24
FB2-1	58,396	BFRP bar was pull out without obvious cracks on the concrete	4.89
FB2-2	300,000	Tensile failure of BFRP bar, the concrete has no obvious cracks	–
FB3-1	444	BFRP bar was pull out with cracks on the concrete	2.87
FB3-2	–	–	–
FB4-1	5846	BFRP bar was pull out with cracks on the concrete	4.26
FB4-2	49,133		–
FB5-1	31	BFRP bar was pull out with cracks on the concrete	2.12
FB5-2	–	–	–

to conduct fatigue test with more than three specimens, while considering the experiment work and time consuming, the authors select 2 specimens according to literatures (El Refai 2013; Shi et al. 2017). The results of specimens under cyclic loads with different stress levels are listed in Table 5.

4 Analysis of Rib Parameters Under Mono-tensile Load

4.1 Analysis of Rib Shape

As the bond–slip curves of BFRP bars with round ribs (B-r), rectangular ribs (B-rec), cross-winding ribs (B-cw) and spiral-winding ribs (B-sw) appear to have similar tendencies, one group of bond–slip curves was analyzed (Fig. 6) for each type of bar, to understand the interaction between different types of ribbed BFRP bars and concrete. In addition, comparisons of the bond strength (the maximum bond stress in bond–slip curve) and deformability between steel rebars (S) and BFRP bars have been carried out.

In terms of the maximum bond stress (Fig. 7), the round-ribbed BFRP bar possesses a bond strength of

**Fig. 6** Bond (τ)–slip (s) curves.

15.8 MPa, which is 29.5% larger than that of steel rebar (12.2 MPa). The average strength of rectangular-ribbed, cross-winding-ribbed and spiral-winding-ribbed BFRP bars is 80.6% that of the round rib type. However, the slip at the maximum bond stress of steel rebar is smaller than B-cw and B-sw, but is 25% larger than B-r and B-rec. This could be attributed to the fact that the steel rib has a larger stiffness as compared to glued ribs (B-cw and B-sw). In addition, the machined rectangular-ribbed bar experiences the lowest bond strength, while its slip is relatively small. This is attributed to the discontinuous fiber having a wider rib contact area with the concrete matrix as compared to other rib shapes.

For the residual stage, the bond strength of all the BFRP bars exhibits cyclic attenuation against the slip. The round-ribbed BFRP bar finally decreases to the strength of 7.04 MPa, then the curve experiences cyclic attenuation. In contrast, those of steel rebar gradually decay, and become linear after a rapid drop of bond strength. Such differences in the residual bond behavior are attributed to the fact that the engaged tooth between the steel rib and concrete experiences failure, while the ribbed BFRP bars still possess certain mechanical interaction with partly engaged teeth. In addition, the residual strength is considered as an adequate development of bond ductility, which exhibits excellent energy consumption performances in seismic design.

It could be concluded that with reasonable design, the round-ribbed BFRP bars would exhibit reliable bond behavior in terms of bond stress, slip, and residual bond ductility, and thus the following optimization analysis is conducted based on the round-ribbed BFRP bars.

4.2 Analysis of Rib Spacing

An analysis of the rib spacing is carried out to evaluate the bond strength and corresponding slip against the rib spacing. As shown in Fig. 8a, the bond strength

Liu *et al. Int J Concr Struct Mater*   (2020) 14:19

Page 9 of 15

Fig. 7 Comparison of bond behavior between BFRP bars and steel rebar.
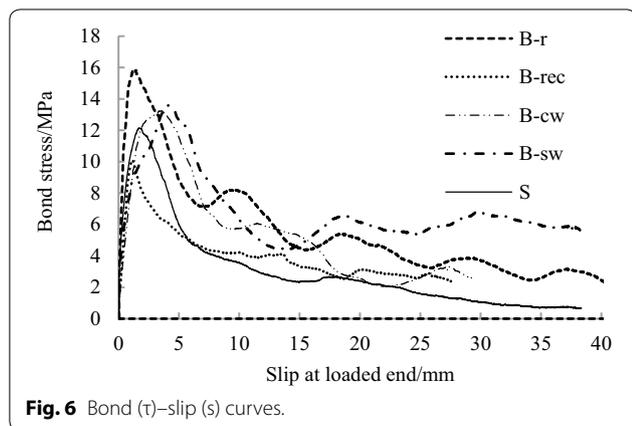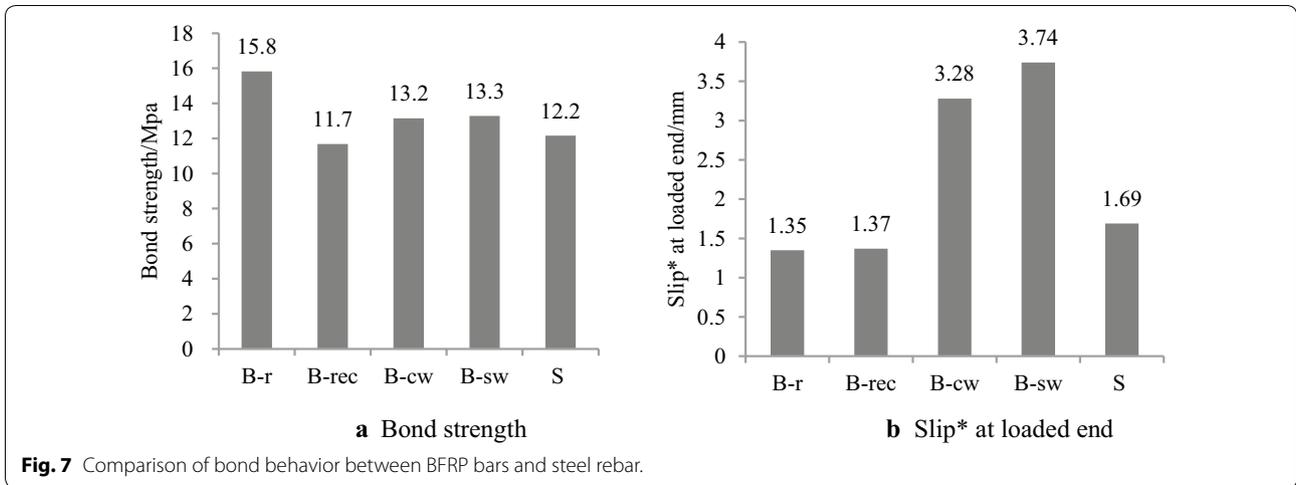
first experiences an increase, and then decreases while the slip keeps increasing. For the given space/diameter of 1, the bond strength (19.74 MPa) improves by 19.7% and 55.8% as compared to space/diameters of 0.5 and 1.5, respectively. Such a phenomenon is caused by the fact that, with an increase in rib spacing, the number of interlocking teeth for the BFRP bar against concrete will decrease as the bond length remains constant, and thus the total mechanical interlock effect will be weakened. Meanwhile, adequate slip is needed to develop sufficient bond resistance (Fig. 8b). However, a large slip can generate large cracks in structures and should be avoided at the serviceability state. The average slip with a rib spacing of 12 mm was 3.77 mm, which is larger than 2.44 mm (corresponding to rib spacing/diameter of 0.75) and smaller than that of 3.87 mm (corresponding to rib spacing/diameter of 1.5). Therefore, a space/

diameter of 1 is suggested, with the maximum bond strength and moderate slip.

4.3 Analysis of Rib Width
The bond strength and corresponding slip against the rib width are exhibited in Fig. 9. The bond strength initially decreases by 7.1%, and then increases 1.1% with the increase in rib width. Correspondingly, the slip reaches the maximum value at the width/diameter of 0.2. No obvious law for width against strength or slip could be obtained, but a width/diameter of 0.2 is suggested to be avoided in practice.

4.4 Analysis of Rib Height
Bond behavior at different rib heights is also estimated quantitatively, and the results are shown in Fig. 10. With an increase of rib height, the bond strength decreases,

Fig. 8 Bond strength and corresponding slip of BFRP bar against rib spacing.

Fig. 9 Bond strength and corresponding slip against rib width.
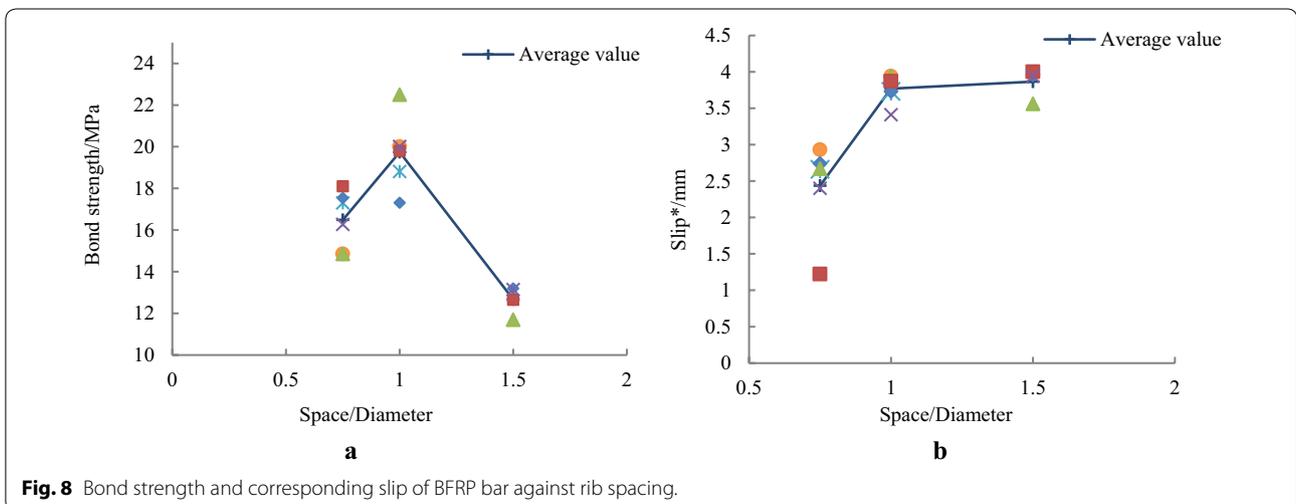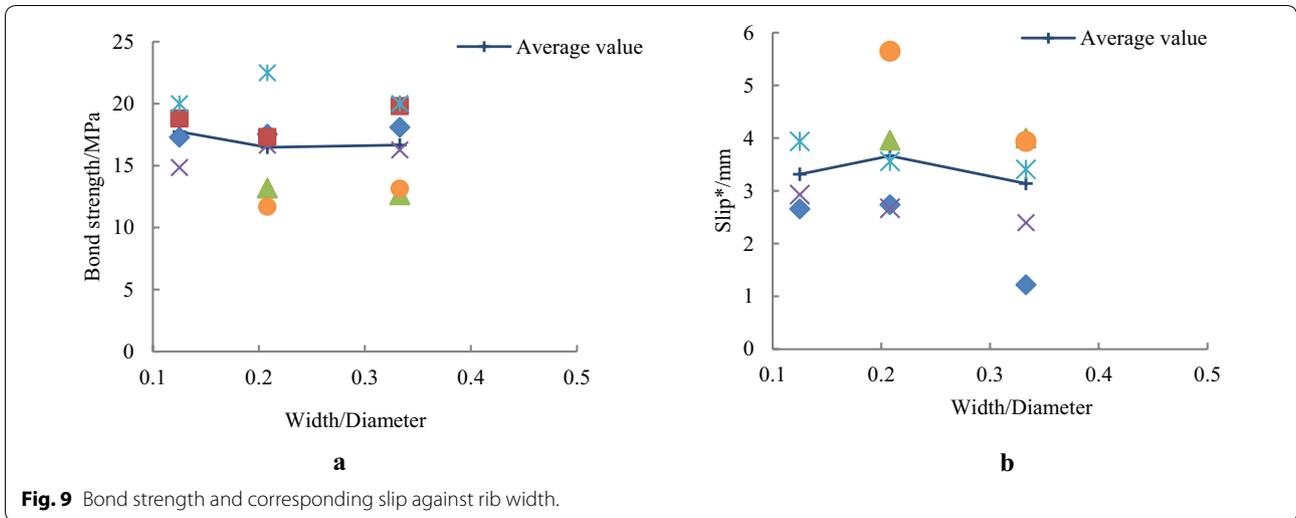
while the slip increases. In fact, when the rib height increases to a certain value, the rib will experience failure first as compared to concrete, with such failure being caused by excessive mechanical interlocking.

Thus, a parameter of a rib spacing/diameter of 1 is recommended in this study, whereas the suitable width and height still require further investigations. In addition, a BFRP bar with a rib spacing of 12 mm, a rib width of 2.5 mm, and a rib height of 1.08 mm possesses the highest strength, and a BFRP bar with these rib parameter is selected for further study on its fatigue behavior.

4.5 Analysis of Relative Rib Area

Literature (Darwin and Graham 1993) indicated that, the magnitude of the increase on bond strength increases with an increase in the relative rib area. This did not occur in this study on BFRP bar. As shown in Fig. 11,

BFRP bars with rib heights of 0.84 mm and 1.08 mm reach the maximum bond strength with relative rib area of 0.07 and 0.09 respectively, and then the bond strength decreases with the increase of R_r. The difference may be attributed to the shear failure at surface layer of BFRP bars, and further study is needed.

4.6 Bond–Slip Constitutive Model

4.6.1 Establishment of Bond–Slip Constitutive Model

The Bertero–Popov–Eligehausen (BPE) model was first proposed by Eligehausen in 1983 (Rossett et al. 1995) and was applied to concrete structures reinforced with FRP by Popov and Bertero (Eligehausen et al. 1983). Then, it was widely adopted in the numerical analysis of interfaces between deformed steel rebars and concrete, and later, it was successfully applied in analysis of FRP-reinforced structures. Despite the numerous formulations and models proposed in the past for FRP bars, such as

Fig. 10 Bond strength and corresponding slip against rib height.

Liu *et al. Int J Concr Struct Mater*   (2020) 14:19

Page 11 of 15

Fig. 11 Bond strength versus relative rib area.

Fig. 12 Comparison of experimental data and existing models.
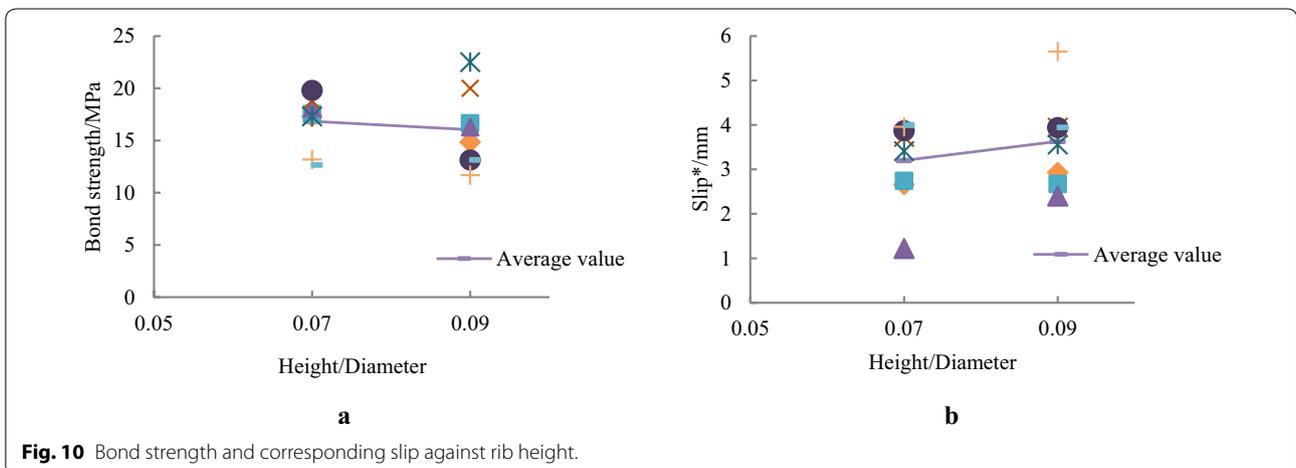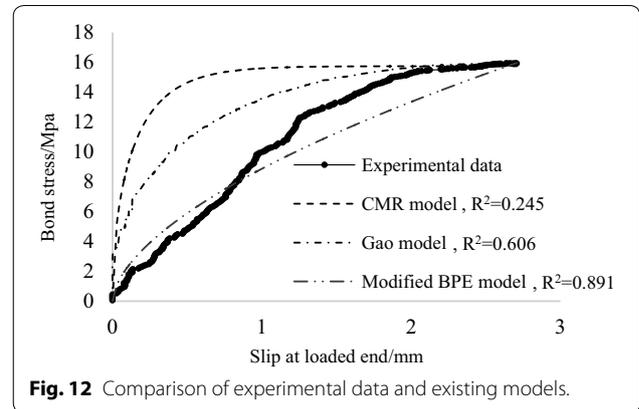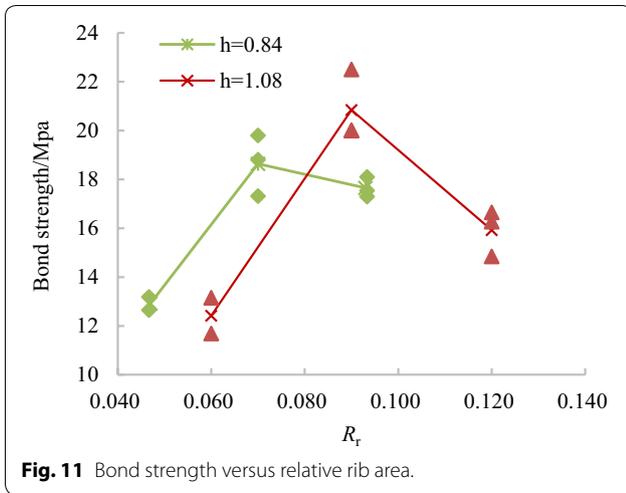
the BPE model (Eligehausen et al. 1983), modified BPE model (Cosenza et al. 1997) and the Cosenza–Manfredi–Realfonzo (CMR) model (Cosenza et al. 1995), these efforts focused on theoretical modeling, while ignoring the considerations of both explicit and physical concepts. Based on previous models, Gao et al. (2003) proposed a continuous curve model with an infinite slope at the origin point, and zero at the ultimate slip. The model was developed with a mathematical derivation with physical meanings, whereas its expression of the descending branch was complex. Furthermore, a continuous bond–slip model with four branches for GFRP/steel wire composite rebars was proposed by Hao et al. (2009). Xue et al. (2016) propose a whole model of the bond–slip for GFRP bars with four branches, i.e. a linearly ascending branch, a ascending branch of the BPE Model, a linearly descending branch and a residual branch in the shape of the sinusoid.

Nevertheless, a constitutive model for BFRP bars still needs to be explored with additional effort, as two main deficiencies exist in previous models. First, the CMR model and Gao's model are not suitable for a BFRP bar, as the ascending branch cannot be correctly fitted, as shown in Fig. 12. For the residual stage, the model of Gao adopts four parameters to describe the residual bond strength, whereas the expression is complex. In fact, residual bond strength is not recommended to be utilized in terms of bond design, while the residual stage exhibits development of bond ductility. Therefore, an optimized bond–slip constitutive model for a BFRP bar with explicit mathematical meaning is proposed, where a linearly descending branch was adopted to characterize the residual branch (shown in Fig. 13). Compared to Xue's model, the first three branches are

similar whereas the residual branch is calibrated form the perspective of energy conservation.

As indicated in Fig. 13a, the OA segment is defined as the micro-slip stage, where the bond strength τ_1 is linear, up to a bond slip of s_1. Then, the τ–s curve gradually turns non-linear, and the ascending branch of AB adopts the expression of the modified BPE model. The descending segment of BC was simulated approximately linearly. In terms of energy conservation at the residual segments, the CD segment adopts a simplified linear model whose envelope area equals the experimental result.

The expressions for the proposed bond–slip are listed as Eq. 2 to Eq. 5.

$$\text{Micro-slide section} \quad \tau = \frac{\tau_1}{s_1}s \quad (s \le s_1) \tag{2}$$

$$\text{Slide section} \quad \tau = (\tau_2 - \tau_1)\left(\frac{s - s_1}{s_2 - s_1}\right)^\alpha + \tau_1 \quad (s_1 < s \le s_2) \tag{3}$$

$$\text{Descending section} \quad \tau = \tau_2 + (\tau_3 - \tau_2)\left[\frac{s - s_2}{s_3 - s_2}\right]$$
$$(s_2 < s \le s_3) \tag{4}$$

$$\text{Residual section} \quad \tau = \tau_3 + (\tau_4 - \tau_3)\left[\frac{s - s_3}{s_4 - s_3}\right] \quad (s > s_3) \tag{5}$$

In the above, τ_1, τ_2, τ_3 and τ_4 are the bond strengths corresponding to points A, B, C, and D, respectively, s_1, s_2, s_3 and s_4 are the corresponding slips, respectively, and all of the them must be calibrated based on the experimental results. A proposed bond–slip model for B-r-1.08-9-2.5 is plotted using parameters in Table 6. Comparison of proposed model and experimental data during the whole slip process is shown in Fig. 13b.

Liu *et al. Int J Concr Struct Mater*   (2020) 14:19

Page 12 of 15

Fig. 13 **a** Bond–slip constitutive law for BFRP bar in concrete and **b** comparison of proposed model and experimental data during the whole slip process.
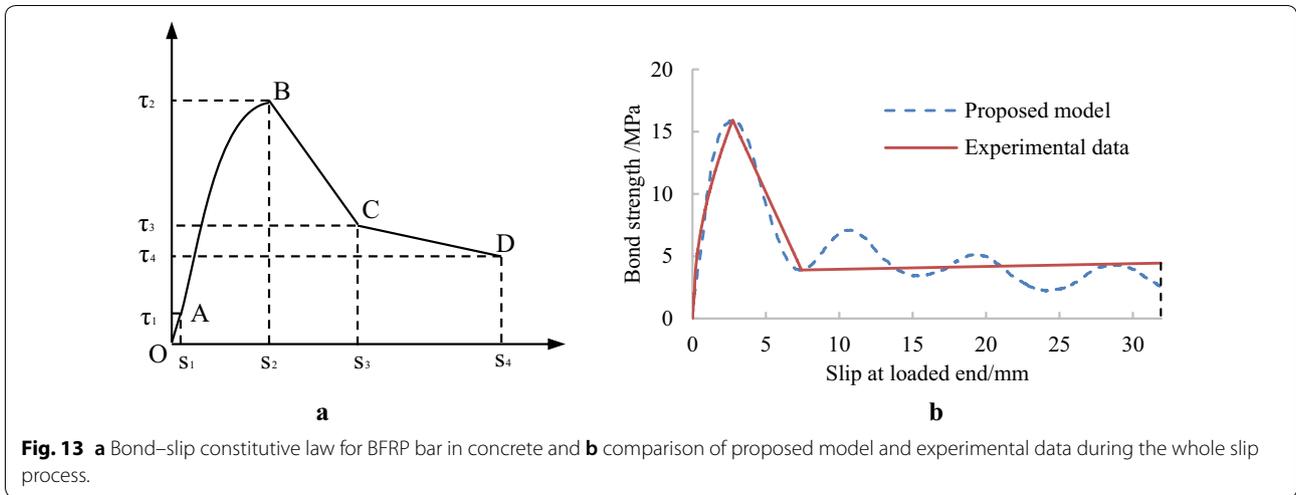
Table 6 Data of boundary point and fit value of parameters.

Specimen number	Experimental data of boundary points								Parameter α	Regression coefficient R^2
	A		B		C		D			
	s_1	τ_1	s_2	τ_2	s_3	τ_3	s_4	τ_4		
	mm	MPa	mm	MPa	mm	MPa	mm	MPa		
B-r-0.84-9-1.5	0.14	3.36	2.62	16.23	8.10	3.91	57.3	2.87	0.49	0.920
B-r-0.84-9-2.5	0.19	3.54	2.68	15.32	7.80	3.85	60.4	1.33	0.31	0.931
B-r-0.84-9-4	0.12	6.10	1.66	16.07	6.38	4.57	53.8	1.23	0.48	0.933
B-r-0.84-12-1.5	0.55	12.95	2.94	23.46	9.51	7.20	55.1	6.13	0.60	0.936
B-r-0.84-12-2.5	0.51	11.82	3.47	28.26	10.58	9.83	53.2	9.49	0.46	0.930
B-r-0.84-12-4	0.29	6.95	2.86	21.10	9.89	7.80	54.7	7.49	0.70	0.936
B-r-0.84-18-2.5	0.54	4.75	4.30	12.28	17.60	1.52	49.3	4.75	0.39	0.944
B-r-0.84-18-4	0.57	3.15	4.03	10.83	15.86	1.63	46.3	2.81	0.70	0.906
B-r-1.08-9-1.5	0.06	3.35	3.15	14.54	7.95	3.09	31.6	5.60	0.55	0.917
B-r-1.08-9-2.5	0.14	2.14	2.74	15.94	7.44	3.88	31.9	4.44	0.58	0.936
B-r-1.08-9-4	0.10	4.07	1.42	15.81	7.06	7.12	50.5	0.46	0.47	0.931
B-r-1.08-12-1.5	0.57	7.63	4.21	21.09	11.59	5.12	31.5	9.17	0.40	0.940
B-r-1.08-12-2.5	0.57	5.35	3.46	22.53	10.41	4.29	45.2	5.55	0.58	0.944
B-r-1.08-12-4	0.62	5.02	3.41	20.41	10.11	4.68	31.5	8.55	0.57	0.932
B-r-1.08-18-2.5	0.39	2.58	5.48	10.85	16.35	1.16	60.1	3.19	0.44	0.950
B-r-1.08-18-4	0.36	2.63	4.21	13.00	17.13	2.30	60.3	3.11	0.50	0.921
B-rec-0.84-12-4	0.37	3.51	1.07	11.69	7.13	5.81	50.5	1.01	0.39	0.911
B-cw-0.84-12-4	0.23	4.51	3.12	14.11	7.53	7.58	39.0	3.41	0.45	0.956
B-sw-0.84-12-4	0.39	5.65	4.98	13.62	14.58	4.72	37.9	1.50	0.60	0.921

4.6.2 Fitting of the Bond–Slip Constitutive Law

The data of the boundary points A, B, and C (shown in Table 6) are obtained from the pull-out tests, whereas D is determined by the area under the residual section of the graph. To obtain the parameter α in Eq. 3, curve fitting is carried out on the experimental data with Origin (a professional data processing software).

The regression coefficient R^2 of the OABC segment is shown in Table 6.

5 Analysis of Fatigue Behavior
5.1 Prediction of Fatigue Life by Data Fitting

An S–N curve was adopted to predict the fatigue life, with a linear scale of the cycles of corresponding stress

Liu *et al. Int J Concr Struct Mater* (2020) 14:19

Page 13 of 15

levels on the vertical axis, and a logarithmic scale of the cycles on the horizontal axis. The approximation line was drawn by a least square fit by the data in Table 5, and the static strength with 1 cycle. For three groups of bars, with rib spacing of 12 mm, rib width of 2.5 mm, and rib height of 1.08 mm, the static strengths are 22.1 MPa, 22.5 MPa, and 23.0 MPa, respectively, corresponding to stress levels of 0.98, 1.00, and 1.02, respectively. The data of the specimen without failure in the fatigue test is not included in the curve fitting, and the other data show a relatively low scattering. The prediction obtained by Eq. (6) and the prediction of the S−N fatigue curve are shown in Fig. 14.

$$S = -0.026 \ln(x) + 0.9662 \tag{6}$$

The slope of the curve characterizes the degradation rate of the expected fatigue life. The proposed equation for predicting fatigue life has a regression coefficient of $R^2 = 0.880$. Substituting $N = 2 \times 10^6$ into Eq. 6, the stress level for 2 million cycles is calculated to be 0.589, which is 1.8% smaller than the experimental value of 0.6. The discrete data is acceptable, and the model is valid for prediction of fatigue life.

5.2 Slip Analysis Under Cyclic Loads

Bond behavior under cyclic loading was mainly characterized by slip, stress level (S_l), and number of cycles (N), as shown in Fig. 15. The slip* of mono-tensile specimen (B-r-1.08-12-2.5) was compared with that of fatigue specimen with the same bar pattern (rib spacing of 12 mm, height of 1.08 mm and width of 2.5 mm). The ratio of fatigue slip to mono-tensile slip at the loaded end was adopted to evaluate the increased slip for specimens under cyclic loads. N/N_f was adopted to normalize slip against the cycles, where N_f was the fatigue life.
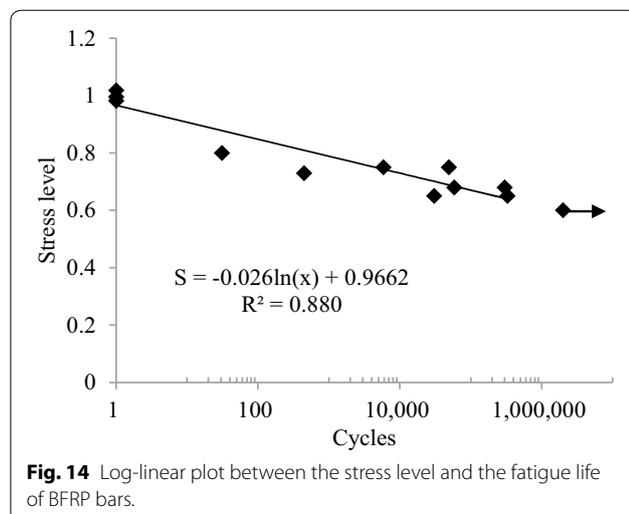
Fig. 14 Log-linear plot between the stress level and the fatigue life of BFRP bars.

As shown in Fig. 15b, the slips under cyclic loads are much larger than those under mono-tensile loads (Fig. 15a) with the largest ratio at 203%, and are attributed to the accumulation of damage during the cyclic process. For the stress levels of 0.73, 0.75, and 0.8, the slip ratios are smaller than that of 0.65 and 0.68. According to the aforementioned failure modes, the small slips were attributed to the splitting of concrete occurring at high stress levels, where the over-developed bearing resistance causes early pull-out of the BFRP bar. In particular, at the stress level of 0.8, the slip ratio could only reach 74%, with a fatigue life of 31 cycles.

As indicated in Fig. 15c, the development of slip under cyclic loads is classified into three stages. The first stage ranges from the fatigue life of 0% to 10%, where the slip increases linearly. From the fatigue life of 10% to 90%, the slip developed steadily. At the last 10% of the fatigue life, the slip increased sharply, and the third stage was terminated until the pull-out of the BFRP bar. This phenomenon could be expressed by the model shown in Fig. 15d.

Under lower cyclic loads, the failure of the chemical bond and friction between the rib and concrete are the dominant factors causing the slip increase at the first stage. With an increase in the number of cycles, mechanical interlocking becomes the primary means of stress transfer and the rib is worn away repeatedly; this is attributed to the stable increase of slip during the second stage. With the accumulation of rib damage, the bar is pulled out abruptly when the rib is eliminated to a certain extent, indicating complete failure of the specimen.

In fact, a large number of micro-cracks were generated during the hydration of concrete and were distributed on the interface of cement and aggregate. Under a high stress level, the concrete around the bar is separated into several wedges by the rib of the bar, and the stress at the top of the cracks was relatively large. Micro-cracks develop rapidly when the stress of wedges exceeds the cohesive strength of concrete. When the development of micro-cracks reaches the saturation state, the wedge starts to crush, and the slip gains a quick increase, as exhibited in the first stage. Afterwards, micro-cracks turn into macro cracks, and the slip enters a stable stage. With the increase of cycles, the wedges crush quickly and steadily with the accumulation of damage. The BFRP bar is pulled out when the last few wedges are crushed.

6 Conclusions

In this study, the bond behavior between a BFRP bar and concrete was investigated, based on monotonic tests and cyclic tests. The bond behavior and the influence of

Liu *et al. Int J Concr Struct Mater*   (2020) 14:19

Page 14 of 15

Fig. 15 The slip under cyclic load of round ribbed bar with rib spacing of 12 mm, width of 2.5 mm and height of 1.08 mm.
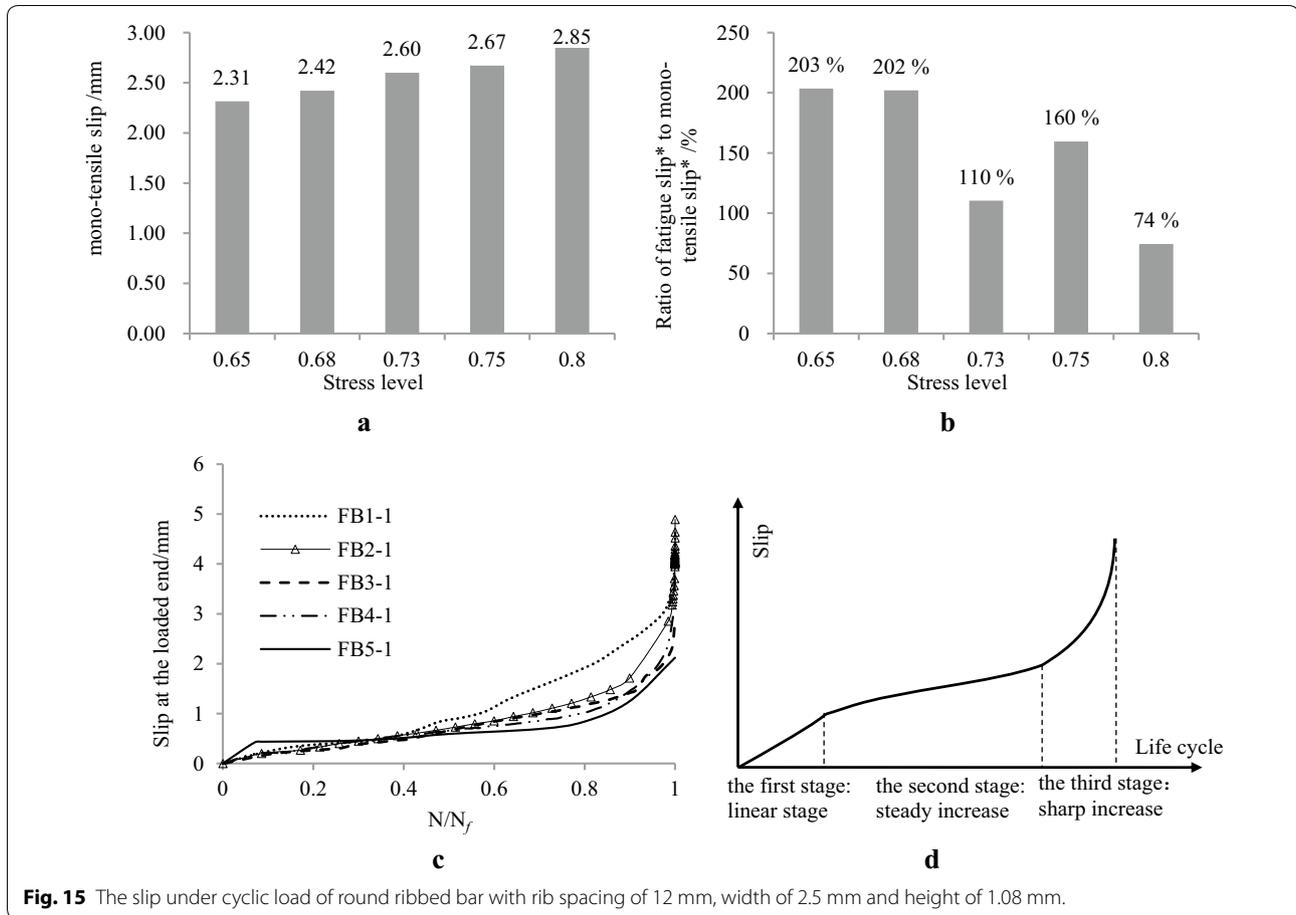
the rib parameters were analyzed, and then an analytical model of bond–slip behavior was proposed for the BFRP bar. Moreover, the fatigue behavior of a selected BFRP bar was evaluated. The following conclusions were drawn.

1. The failure modes of structures reinforced with BFRP bar under the mono-tensile test could be classified as pull-out failure and split failure, while those of the cyclic tests can be categorized as pull-out of the bar, split of the concrete, and fracture of the bar. The first two types of failure modes occur more abruptly under cyclic tests as compared to those under mono-tensile loads.

2. In the analysis of rib parameters, the round-ribbed BFRP bar exhibits the largest bond strength as compared to other rib shapes. In addition, a rib spacing/diameter of 1 is recommended, while avoiding a width/diameter of 0.2. A rib spacing of 12 mm and a rib width of 2.5 mm are recommended for maximum bond strength and moderate slip.

3. The bond–slip constitutive model dedicated to the BFRP bar was proposed with four main stages, i.e., micro-slip, slip, descending, and residual stages. The parameter fitting in the proposed model shows reasonable agreement between numerical and actual values at the first three stages. For the residual stage, bond ductility is the focus, and it is characterized linearly based on conservation of energy.

4. The fatigue life is predicted by an S–N fatigue curve and an equation with a regression coefficient of $R^2 = 0.880$; it reaches high accuracy at 2 million cycles, with an error of 1.8% as compared to that of the experimental test. In addition, the development of slip under cyclic loads was classified into three stages, providing an alternate way to understand the failure mechanism.

Liu *et al. Int J Concr Struct Mater*   (2020) 14:19

Page 15 of 15

Availability of data and materials
All data analyzed during this study are included in this published article.

Competing interests
The authors declare that they have no competing interests.

Author details
[1] College of Field Engineering, Army Engineering University of PLA, Nanjing 210007, Jiangsu, China. [2] Key Laboratory of C & PC Structures Ministry of Education, Southeast University, Nanjing 210096, Jiangsu, China. [3] College of Architectural Engineering, Zhongyuan University of Technology, Zhengzhou 450007, Henan, China.

References
Achillides, Z., & Pilakoutas, K. (2004). Bond behavior of fiber reinforced polymer bars under direct pullout conditions. *Journal of Composites for Construction, 8*(2), 173–181.

ACI 440.3R-04. (2004). *Guide Test Methods for Fiber-Reinforced Polymers (FRPs) for Reinforcing or Strengthening Concrete Structures, ACI Committee 440*, American Concrete Institute.

Barena, M., Torres, L., Turon, A., et al. (2009). Experimental study of bond behaviour between concrete and FRP bars using a pull-out test. *Composites Part B Engineering, 40*(8), 784–797.

Caro, M., Jemaa, Y., Dirar, S., & Quinn, A. (2017). Bond performance of deep embedment FRP bars epoxy-bonded into concrete. *Engineering Structures, 147,* 448–457.

Chaallal, O. (1993). Pullout and bond of glass-fibre rods embedded in concrete and cement grout. *Materials and Structures, 26,* 167–175.

Chaallal, O., & Benmokrane, B. (1993). Pullout and bond of glass-fibre rods embedded in concrete and cement grout. *Materials and Structures, 26*(3), 167–175.

Cosenza, E., Manfredi, G., Pecce, M., et al. (1999). Bond between glass fiber reinforced plastic reinforcing bars and concrete—experimental analysis. In: *Proceedings, FRPRCS-4, 4th international symposium on fiber reinforced polymer reinforcement for reinforced concrete structures*. pp. 347–358.

Cosenza, E., Manfredi, G., Realfonzo, R. (1995). Analytical modeling of bond between FRP reinforcing bars and concrete//Taerwe L. Non-metallic (FRP) reinforcement bars for concrete. In: *Proceedings of the 2nd international RILEM symposium (FRPRCS-2), Ghennt, London, England*. pp. 164–179.

Cosenza, E., Manfredi, G., & Realfonzo, R. (1997). Behavior and modeling of bond of FRP bars to concrete. *Journal of Composites for Construction, 1*(2), 40–51.

Cox, J.V., Guo, J. (1999). Modeling stress state dependency of bond behavior of fiber reinforced polymer tendons. In: *International symposium on fiber reinforced polymer reinforcement for reinforced concrete structures*. pp. 791–805.

Cox, J.V., Herrmann, L.R. (1992). Confinement stress dependent bond behavior, part II: A two degree of freedom plasticity model. In: *Proceedings of the international conference on bond in concrete*. pp. 11–11.

Darwin, D., & Graham, E. K. (1993). Effect of deformation height and spacing on bond strength of reinforcing bars. *ACI Structural Journal, 90*(6), 646–657.

El Refai, A. (2013). Durability and fatigue of basalt fiber-reinforced polymer bars gripped with steel wedge anchors. *Journal of Composites for Construction, 17*(6), 04013006.

Eligehausen, R., Popov, E.P., Bertero, V.V. (1983). *Local bond stress-slippage relationships of deformed bars under generalized excitations*. Rep. No. 83/23, Earthquake Engineering, Res, Ctr, (EERC), Univ. of California, Berjekey. pp. 162–169.

Gao, D., Zhu, H., & Xie, J. (2003). The constitutive models for bond slippage relation between FRP bars and concrete. *Industrial construction, 33*(7), 41–43.

Hao, Q., Wang, Y., Hou, J., et al. (2009). Bond-slippage constitutive model between GFRP/Steel wire composite bars and concrete. *Engineering Mechanics, 26*(5), 62–72.

Hollaway, L. C. (2010). A review of the present and future utilization of FRP composites in the civil infrastructure with reference to their important in-service properties. *Construction and Building Materials, 24*(12), 2419–2445.

Japan Society of Civil Engineering. (1995). *Test method for tensile properties of continuous fiber reinforcing materials, JSCE-E 531, Tokyo*.

JSCE (Japan Society of Civil Engineers). (1995). *Test method for tensile fatigue of continuous fiber reinforcing materials. JSCR-E 535, Tokyo*.

Keller, T. (2003). *Use of fibre reinforced polymers in bridge construction*. Zurich: IASBSE-AIPC-IVBH.

Lopresto, V., Leone, C., & Iorio, I. D. (2011). Mechanical characterization of basalt fibre reinforced plastic. *Composites: Part B, 42,* 717–723.

Malvar, L. J., Cox, J. V., & Cochran, K. B. (2003). Bond between carbon fiber reinforced polymer bars and concrete. I: Experimental study. *Journal of Composites for Construction, 7*(2), 154–163.

Rossett, V. A., Galeota, D., & Giammatted, M. M. (1995). Local bond stress-slippage relationships of glass fiber reinforced plastic bars embed in concrete. *Material and structure, 28,* 340–344.

Saito, M. (2002). Carbon fiber composites in the Japanese Civil Engineering Market: Conventional uses and developing products. *SAMPE Journal, 38*(5), 20–25.

Shi, J., Wang, X., Wu, Z., & Zhu, Z. (2017). Fatigue behavior of basalt fiber-reinforced polymer tendons under a marine environment. *Construction and Building Materials, 137,* 46–54.

Tekle, B. H., Khennane, A., & Kayali, O. (2017). Bond behavior of GFRP reinforcement in alkali activated cement concrete. *Construction and Building Materials, 154,* 972–982.

Torres, J. P., Hoto, R., & Andrés, J. (2013). Manufacture of green-composite sandwich structures with basalt fiber and bioepoxy resin. *Advances in Materials Science and Engineering, 2013,*, 214506.

Wu, Z., Wang, X., & Iwashita, K. (2007). State-of-the-art of advanced FRP applications in civil infrastructure in Japan. *Composites and Polycon, 37,* 1–17.

Xue, W., Yang, Y., Zheng, Q., et al. (2016). Modeling of bond of sand-coated deformed glass fibre-reinforced polymer rebars in concrete. *Polymers and Polymer Composites, 24*(1), 45–56.

Publisher's Note
Springer Nature remains neutral with regard to jurisdictional claims in published maps and institutional affiliations.